# CB1 receptor binding sites for NAM and PAM: A first approach for studying, new *n*-butyl-diphenylcarboxamides as allosteric modulators

Francesca Gado [a], Costanza Ceni [a,c], Rebecca Ferrisi [a], Giulia Sbrana [a], Lesley A. Stevenson [b], Marco Macchia [a], Roger G. Pertwee [b], Simone Bertini [a], Clementina Manera [a,*], Gabriella Ortore [a,*]

[a] *Department of Pharmacy, University of Pisa, 56126 Pisa Italy*
[b] *School of Medicine, Medical Sciences and Nutrition, Institute of Medical Sciences, University of Aberdeen, AB25 2ZD Aberdeen, Scotland, UK*
[c] *Doctoral school in Life Sciences, University of Siena, Via Aldo Moro 2, 53100, Siena, Italy*

ABSTRACT

The development of cannabinoid receptor type-1 (CB1R) modulators has been implicated in multiple pathophysiological events ranging from memory deficits to neurodegenerative disorders among others, even if their central psychiatric side effects such as depression, anxiety, and suicidal tendencies, have limited their clinical use. Thus, the identification of ligands which selectively act on peripheral CB1Rs, is becoming more interesting. A recent study reported a class of peripheral CB1R selective antagonists, characterized by a 5-aryl substituted nicotinamide core. These derivatives have structural similarities with the biphenyl compounds, endowed with CB2R antagonist activity, previously synthesized by our research group. In this work we combined the pharmacophoric portion of both classes, in order to obtain novel CBR antagonists. Among the synthesized compounds rather unexpectedly two compounds of this series, **C7** and **C10**, did not show the radioligand ($[^3H]$CP55940) displacement on CB1R but increased binding ($\sim$ 150%), suggesting a possible allosteric behavior. Computational studies were performed to investigate the role of these compounds in CB1R modulation. The analysis of their binding poses in two different binding cavities of the CB1R surface, revealed a preferred interaction with the experimental binding site for negative allosteric modulators.

## 1. Introduction

In the last twenty-five years, the endocannabinoid system (ECS) has emerged as a fundamental neuromodulatory system, involved in the regulation of several physiological and pathological processes. (Lu and Mackie, 2016) It is formed by endocannabinoids (eCBs) anandamide (AEA) and 2-arachidonyl-glycerol (2-AG), enzymes responsible for their synthesis and degradation, including fatty acid amide hydrolase (FAAH) and monoacylglycerol lipase (MAGL), hydrolyzing enzymes of AEA and 2-AG respectively, and cannabinoid receptors (CBRs) type-1 (CB1R) and type-2 (CB2R). (Hu and Mackie, 2015) Generally, CB1R is mainly located in CNS, modulating many physiological functions, such as memory, cognition, motor coordination, food intake and pain, (Pertwee et al., 2010) but its expression has also been detected in peripheral tissue, including pancreas, liver and adipose cells, (Nagappan et al., 2019) taking part in the regulation of metabolic processes. (Lipina et al., 2016; Muller et al., 2017) Indeed, CB1R antagonist lead to the reduction of

hyperglycemia, lipogenesis, dyslipidemia and insulin resistance, decreasing also body weight and appetite, (Rubio et al., 2007; Samat et al., 2008) resulting in a promising approach for the treatment of obesity. However, central psychiatric side effects such as depression, anxiety and suicidal tendencies, limited their clinical use. (Moreira et al., 2009; Blasio et al., 2013) In the last years, it was reported that beneficial anti-obesity effects could be especially mediated by peripheral CB1R. (Nogueiras et al., 2008; Cluny et al., 2010; Han et al., 2019) Even if the exact mechanism has not been completely elucidated yet, macrophage CB1R seems to play a key role in the regulation of adipose tissue inflammation, through the activation of NLRP3 inflammasome pathways. (Han et al., 2019) Thus, the identification and the development of antagonists, able to selectively act on peripheral CB1R, could represent a good strategy to avoid the central psychiatric side effects, arising from central CB1R stimulation.

In this context, a recent study reported a class of peripheral CB1R antagonists characterized by a 5-aryl substituted nicotinamide core of

general structure **A** (Fig. 1). (Röver et al., 2013) This series was developed to obtain novel anti-obesity agents, which might have therapeutic potential with minimal central side effects. Unfortunately, all the new molecules characterized by a markedly reduced brain exposure were revealed to have no significant effect on body weight. (Röver et al., 2013) However, this scaffold is nevertheless to be considered interesting for developing novel peripheral CB1R antagonists that could provide potential therapeutic benefits.

These derivatives present structural similarities with some biphenylic carboxamides-based compounds of general structure **B** (Fig. 1) endowed with a CB2R antagonist activity, resulting to be potentially useful as a pharmacological "tool" to study the role of CB2R in physiopathological conditions. (Bertini et al., 2015)

In this work, we designed and synthesized compounds of general structure **C** (Fig. 1), with the aim to obtain novel selective antagonists on one of two subtypes of CBRs and to explore the effect of the shift of the n-butyl chain of **B**, related to a CB2R antagonist activity, in position 6, involved in the CB1R antagonism. This modification can highlight key groups involved in the interaction with binding sites of CBRs; furthermore, the N-substitution with both cyclohexanol and cycloheptyl moieties on the same scaffold can investigate the role of the hydroxyl in the selectivity. In particular, the main structural differences of compounds **C** with respect to compounds **A** and **B** are represented by the replacement of the nitrogen atom of **A** with a carbon atom, the shift of the n-butyl chain of **B**, and an amide group with $R_2$ = cycloheptyl or *trans*-2-hydroxycyclohexyl in analogy with the biphenyl derivatives **B** and the nicotinamide derivatives **A** respectively. Finally, in analogy with the biphenyl derivatives **B**, compounds **C** are characterized by H, $OCH_3$ or *F* as substituent of the peripheral aromatic ring ($R_1$), and by a substituent $R_3$ = H, $OCH_3$ in the central aromatic ring.

Summing up, the structural features of the new compounds **C1-C12** are reported in Table 1.

It was hypothesized that the new hybrid compounds could be characterized by antagonist effects towards the CBRs. The main goal of this study was then to define the possible receptor sub-type selectivity towards CBRs. Unexpectedly, the biological assays revealed a different profile of functional activity compared to the previous classes **A** and **B**. In particular two compounds of this series, **C7** and **C10**, increased the CB1R binding of the radioligand CBR unselective agonist [3H]CP55940, suggesting a possible allosteric behavior.

Allosterism is a complex phenomenon, very interesting for modulating receptor activity. Allosteric modulators interact with a receptor's allosteric site(s) which are topographically different from the orthosteric one, and this binding leads to conformational changes that are transmitted to the orthosteric site inducing an increment of the receptor signaling due to increased potency and/or efficacy of orthosteric ligands (positive allosteric modulator, PAM), or to a decrease of the receptor

**Table 1**
Summary of structural features of compounds C.

| Cpd | $R_1$ | $R_2$ | $R_3$ |
| --- | --- | --- | --- |
| **C1** | $OCH_3$ | cycloheptyl | $OCH_3$ |
| **C2** | H | cycloheptyl | $OCH_3$ |
| **C3** | F | cycloheptyl | $OCH_3$ |
| **C4** | $OCH_3$ | cycloheptyl | H |
| **C5** | H | cycloheptyl | H |
| **C6** | F | cycloheptyl | H |
| **C7** | $OCH_3$ | *trans*-2-hydroxycyclohexyl | $OCH_3$ |
| **C8** | H | *trans*-2-hydroxycyclohexyl | $OCH_3$ |
| **C9** | F | *trans*-2-hydroxycyclohexyl | $OCH_3$ |
| **C10** | $OCH_3$ | *trans*-2-hydroxycyclohexyl | H |
| **C11** | H | *trans*-2-hydroxycyclohexyl | H |
| **C12** | F | *trans*-2-hydroxycyclohexyl | H |

signaling with a decrement of potency and/or efficacy of the orthosteric agonist (negative allosteric modulator, NAM). (Gentry et al., 2015) Finally, allosteric modulators can also be a combination of PAM and NAM depending on the signaling output being measured. (Alaverdashvili and Laprairie, 2018)

Allosteric modulators offer the potential to fine-tune the affinity and/or efficacy of the orthosteric ligand in a site-, event-, and orthosteric ligand-specific manner. These intrinsic molecular properties of allosteric modulators are particularly attractive for CB1R modulation, since they could enhance safety and efficacy and circumvent the adverse effects of typical CB1R orthosteric ligands. Moreover, allosteric ligands may alter the signal bias of orthosteric ligands, or display ligand bias themselves, engaging certain signaling interactions (e.g., G proteins) over others (e. g., beta-arrestins). In particular, it's known that CB1R is capable of recruiting beta-arrestins and then the chronic treatment with cannabinoids induce receptor desensitization and internalization, that might lead to tolerance and downregulation of CB1R receptor activity in the brain. Allosteric CB1R ligands have shown to selectively trigger or inhibit specific signal pathways suggesting that allosteric-binding sites represent a promise for the development of strongly biased CB1R ligands.

Computational studies are here performed to investigate the allosteric behavior of **C7** and **C10**, starting with the recent experimental information about NAM binding in CB1R. (Shao et al., 2019) Combining three-dimensional experimental data related to different activation states of CB1R, with mutagenesis results and structure activity relationships of known NAMs and PAMs, we identified a possible site of interaction in CB1R for PAMs. A docking study of **C7** and **C10** in both CB1R allosteric binding sites (the experimental NAM- and the hypothetical PAM- binding sites) revealed for them a preferred interaction with the binding site for NAM.
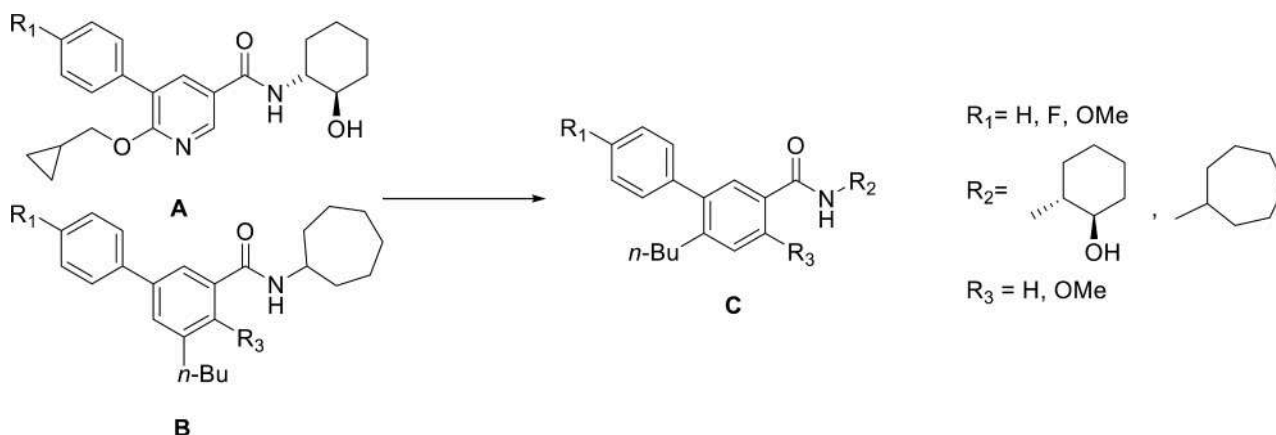


**Fig. 1.** General structure of novel class of compounds **C**.

## 2. Material and methods

### 2.1. Chemistry

A detailed description of compound syntheses and characterization can be found in the supplementary information.

### 2.2. Biological studies

**2.2.1. Compounds used.** All commercial compounds and reagents were purchased from Sigma-Aldrich (Mississauga ON), unless otherwise noted. CP55,940 was purchased from Cayman Chemical (Ann Arbor, MI). All compounds were initially dissolved in DMSO and diluted in a 10% DMSO solution in PBS. Compounds were added directly to cell culture at the times and concentrations indicated at a final concentration of 0.1% DMSO.

**2.2.2. CHO cells.** CHO cells stably transfected with cDNA encoding human cannabinoid CB1Rs or CB2Rs were maintained at 37 °C and 5% $CO_2$ in Gibco Ham's F-12 nutrient mix supplied by Fisher Scientific UK Ltd. that was supplemented with 2 mM L-glutamine, 10% FBS, and 0.6% penicillinstreptomycin, all also supplied by Fisher Scientific UK Ltd. or Canada Ltd., and with the disulfate salt of G418 [(2R,3S,4R,5R,6S)−5-amino-6-{[(1R,2S,3S,4R,6S)−4,6-diamino-3-{[(2R,3R,4R,5R)−3,5-*dihydroxy*-5-*methyl*-4-(*methylamino*)*oxan*-2-*yl*]oxy}−2-hydrox-ycyclohexyl]oxy}−2-[(1R)−1-*hydroxyethyl*]- oxane-3,4- diol; 600 mg/mL] supplied by Sigma-Aldrich UK. All cells were exposed to 5% $CO_2$ in their respective media and were passaged twice a week using non-enzymatic cell dissociation solution. For membrane preparation, cells were removed from flasks by scraping, centrifuging, and then freezing as a pellet at 20 °C until required. Before use in a radioligand binding assay, cells were defrosted, diluted in Tris buffer (50 mM Tris–HCl and 50 mM Tris- base). *h*CB1R and *h*CB2R CHO-K1 cells.

**2.2.3. CB1R and CB2R binding assays.** The assays were carried out with [³H]CP55940 and Tris binding buffer (50 mM Tris–HCl, 50 mM Tri-base, 0.1% BSA, pH 7.4), total assay volume 500 mL. Binding was initiated by the addition of transfected *h*CB1 or *h*CB2 CHO cell membranes (50 mg protein per well). All assays were performed at 37 °C for 60 min before termination by the addition of ice-cold Tris binding buffer, followed by vacuum filtration using a 24-well sampling manifold (Brandel cell harvester; Brandel Inc., Gaithersburg, MD, USA) and Brandel GF/B filters that had been soaked in wash buffer at 4 °C for at least 24 h. Each reaction well was washed six times with a 1.2 mL aliquot of Tris-binding buffer. The filters were oven-dried for 60 min and then placed in 3 mL of scintillation fluid (Ultima Gold XR, Perki- nElmer, Seer Green, Buckinghamshire, U.K.). Radioactivity was quantified by liquid scintillation spectrometry. Specific binding was defined as the difference between the binding that occurred in the presence and absence of 1 mM unlabeled CP55,940. The concentration of [³H]CP55,940 used in our displacement assays was 0.7 nM. The compounds used in this investigation were stored as stock solutions of 10 mM in DMSO, the vehicle concentration in all assay wells being 0.1% DMSO. Each point on each dose-response binding curve represents the mean of data obtained from 6 independent experiments. Each experiment was performed in duplicate for each concentration.

**2.2.4. Functional activity at CB1R.** The GTPγS binding assay was carried out in the presence of [³⁵S] GTPγS (0.1 nM), GDP (30 mM), GTPγS (30 mM), and CHO cell membranes (1 mg/mL) overexpressing *h*CB1Rs. The assay buffer contained 50 mM Tris, 10 mM MgCl₂, 100 mM NaCl, 0.2 mM EDTA, and 1 mM DTT (dithiothreitol) at pH 7.4. Incubations were carried out at 30 °C for 90 min in a total volume of 500 mL. The reaction was terminated by the addition of ice-cold wash buffer

(50 mM Tris and 1 mg/mL BSA, pH 7.4) followed by rapid filtration under vacuum through Whatman GF/B glass-fiber filters (pre- soaked in wash buffer), 24-well sampling manifold (Brandel Cell Harvester; Brandel Inc., Gaithersburg, MD, USA), and Brandel GF/B filters that had been soaked in wash buffer at 4 °C for at least 24 h. Each reaction well was washed six times with a 1.2 mL aliquot of Tris-binding buffer. The filters were oven-dried for 60 min and then placed in 3 mL of scintillation fluid (Ultima Gold XR, PerkinElmer, Seer Green, Buckinghamshire, U.K.). Bound radioactivity was determined by liquid scintillation counting. Basal binding of [³⁵S] GTPγS was determined in the presence of 20 mM GDP and absence of cannabinoid. Nonspecific binding was determined in the presence of 10 mM GTPγS. **C7** was stored as stock solutions of 10 mM in DMSO, the vehicle concentration in all assay wells being 0.1% DMSO. Each point on the CP55,940 graph represents the mean of data obtained from 5 independent experiments. Each experiment was performed in duplicate for each concentration.

### 2.3. Computational studies

**2.3.1 Ligand based study.** The FLAP (Cross et al., 2012; Cross et al., 2010) ligand based screening of **C** compounds was performed using ORG27569 as a NAM template and GAT211 as a PAM template, enriching the set with known allosteric inhibitors showing a positive binding cooperativity with the orthosteric ligand CP55940. So, PSNCBAM-1 had been added as active NAM, and ZCZ011, RTI-371 and JHW007 as active PAM ligands. All **C** compounds had been marked as inactives, excepting **C7, C10** and **C4** as decoys. Ligands have been described in terms of four-point pharmacophoric fingerprints, extracted from the H (mapping the shape), DRY (evaluating hydrophobic affin-ities), N1 and O (mapping H-bond donor and acceptor regions, respec-tively) molecular interaction fields (MIFs) calculated by GRID. (Cross et al., 2010) Flap used the pharmacophoric points to compare and su-perimpose ligands, selecting the most interesting candidates with chemical and structural similarity with ORG27569 (in the NAM model) and GAT211 (in the PAM model). The superimposition had been quantitatively scored by Flap considering the corresponding MIFs sim-ilarity (using single probe or probe-combinations), and the ranking had been analyzed in terms of capability to discriminate active and inactive compounds, measured using the Receiver-Operating Characteristic (ROC) curve as a performance metric.

**2.3.2. Cavities identification.** All CB1 structures available on the PDB website (Berman, 2000) were used for pocket detection. 6KQI (Shao et al., 2019), 5TGZ, (Hua et al., 2016) 5U09, (Shao et al., 2016) 5XRA, 5XR8, (Hua et al., 2017) 6KPG, (Hua et al., 2020) 6N4B (Kumar et al., 2019) crystal structures were checked and all broken residues were mutated using Maestro (Schrödinger Inc. 2009) and optimized. For all structures, excepting those Gi-bound, missing atoms were localized in extracellular or intracellular disordered regions. For 6KPG, (Hua et al., 2020) and in particular 6N4B, (Kumar et al., 2019) missing atoms were scattered also in the TMs exposed to membrane: in TM1 for 6KPG, while TM1, TM4 and TM7 are involved in the 6N4B poorly resolved region. All CB1 structures were imported into FLAP (Cross et al., 2010) by applying the predefined FLAP base filters for pdb files. The FLAPsite (Baroni et al., 2007) algorithm was then applied for the identification of protein cav-ities, using 2,8,2 as the number of additional trials, sensitivity and erosion values, respectively. This non-default parameter setting aimed to force detection of the cavities, our possible binding sites being located on the surface and not in a usual internal pocket. The cavities were compared within all CB1 structures, taking into account the different activation states. The poorly resolved region of 6N4B and 6KQI affected extracellular pockets, a small cavity between the intracellular half of
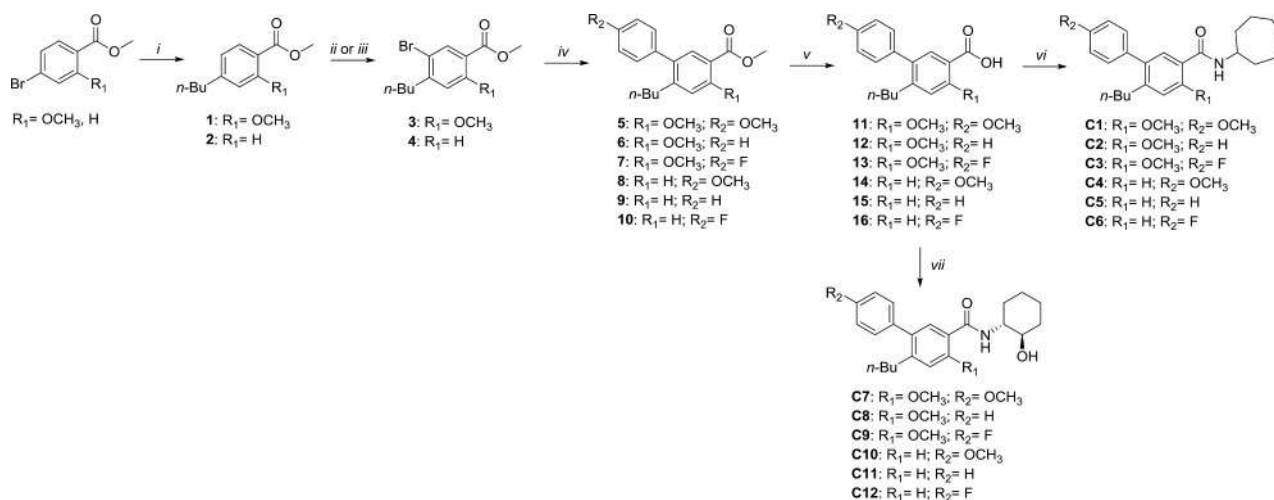
**Scheme 1.** Synthetic pathway for the synthesis of compounds C1-C12.

TM1 and TM7, and the S3 cavity of 6N4B due to Lys232, Val235 and Met238. Since cavity assessment was similar for CB1 structures in the same activation state (5TGZ and 5U09; 5XRA and 5XR8; 6N4B and 6KQI), a blind docking for pocket identification was performed only in 5U09, 5XRA and 6N4B (antagonist-bound, agonist-bound and agonist-Gi-bound) using GOLD, (Verdonk et al., 2003) to compare the results of both programs. For cavity detection, the calculation was set up to enclose all residues within a range of 30 Å from the 5XRA cholesterol. The option "do cavity" has been disabled, to avoid restriction to concave surfaces and to force the identification of cavities. The results were used only to identify, through docking poses, possible binding regions applying enforced settings for pocket detection, and not to produce reliable binding modes. S1, S2 and S3 regions had been highlighted.

**2.3.3 Docking in pockets S1 and S3.** Crystallographic structures 6KQI (Shao et al., 2019) and 6N4B, (Kumar et al., 2019) already refined through Maestro, (Schrödinger Inc. 2009) had been used for docking all **C** compounds and known NAMS (PSNCBAM-1 and ORG27569) and PAMs (ZCZ011, GAT211, RTI-371 and JHW007), selected in view of their binding cooperativity with the orthosteric ligand CP55940. For re-docking the ligand ORG27569 in 6KQI, using the GOLD program, (Verdonk et al., 2003) the region of interest was defined in such a manner that the 6KQI protein contained all the residues within 10 Å of ORG27569 ligand. The "allow early termination" command was deactivated. All ligands were submitted to 40 Genetic Algorithm runs using Chemscore, ASP, PLP and Goldscore fitness functions with flexibility improvement, clustering the output orientations on the basis of an RMSD distance of 1.5 Å. The extra parameters of GOLD were used to permit Lys232, Val235 and Met238 (not completely resolved in crystal structure) free side chain rotations. The default GOLD parameters were used for all other variables. The only fitness function able to re-dock ORG27569 in the 6KQI binding site was PLP, which was used for further calculations. Docking of PAMs was performed in the S3 cavity, selected as a possible alternative allosteric pocket. Since the PAMs effect on the CB1 activation was a positive modulation, their docking was performed in the Gi-bound structure 6N4B, containing two adjacent cholesterol ligands in the S3 cavity. Also in this case, the region of interest was defined in such a manner that the 6N4B protein contained all the residues within 10 Å of cholesterol ligands, and all ligands were submitted to 40 Genetic Algorithm runs using PLP scoring function.

## 3. Results and discussion

**3.1. Chemistry.** The synthesis of compounds **C** is reported in Scheme 1. The commercially available suitable starting material was subjected to a cross-coupling reaction with *n*-butilboronic acid in dry toluene in the presence of bis(dibenzildenacetone)palladium(0), 1,2,3,4,5-pentaphenyl-1-(di-*tert*-butilfosfino)ferrocene and anhydrous $K_3PO_4$ as base, stirred at 100 °C for 12 h to afford the correspondent alkyl derivative (**1** or **2**) which was then purified by flash chromatography. Compound **1** was treated with a solution of bromine in $CHCl_3$ to give compound **3**, while compound **2** with glacial acetic acid, $HNO_3$ (65%), $H_2O$ and $AgNO_3$ to obtain compound **4**. Bromo derivatives underwent a Suzuki cross-coupling reaction in the presence of $Pd(OAc)_2$, $PPh_3$, the suitable boronic acid and aqueous $Na_2CO_3$ (2 M) in dry toluene and methanol, and the mixture was stirred at 85 °C for 12 h to obtain the correspondent 5-substituted compounds (**5**–**10**). After acid hydrolysis of the ester group, carboxylic acid derivatives **11**–**16** went through the last step of the pathway with the formation of the amide group. Thus, compounds **C1**-**C6** were obtained by the reaction of the carboxylic acid derivatives **11**–**16** with $SOCl_2$ and cycloheptylamine in dry $CH_2Cl_2$. In the case of final products **C7**-**C12**, the compounds **11**–**16** were treated with the coupling agent 2-[(1H-benzotri-azole-1-yl)−1,1,3,3-tetramethyl uronium tetrafluoroborate] (TBTU) at 0 °C, in the presence of triethylamine to yield the corresponding activated benzotriazolyl-ester, which reacted with *trans*-2-aminocyclohexanol hydrochloride.

**Reagents and conditions:** *i)* *n*-butilboronic acid, bis(dibenzildenacetone)palladium(0), 1,2,3,4,5- pentaphenyl-1′-(di-*tert*-butilphosphino) ferrocene, $K_3PO_4$, dry toluene, 100 °C, overnight; *ii)* $Br_2$, $CHCl_3$, 0 °C, 1 h; *iii)* $Br_2$, $HNO_3$ (65%), $H_2O$, glacial $CH_3COOH$, $AgNO_3$, r.t., 3 h; *iv)* suitable boronic acid, $Pd(PPh_3)_4$, $Na_2CO_3$ 2 M, dry toluene, MeOH, 85 °C, overnight; *v)* KOH, MeOH, 75 °C, overnight; *vi)* a) $SOCl_2$, reflux, 30 min.; b) cycloheptylamine, dry $CH_2Cl_2$, r.t., overnight; *vii)* *trans*-2-amminocyclohexanol hydrochloride, TBTU, DIPEA, THF, r.t., 4 h.

**3.2. CBR binding properties.** CBRs binding was evaluated by incubating the new compounds (**C1-C6** and **C7-C12**) with membrane preparations obtained from CHO-K1 cells overexpressing *h*CB1R or *h*CB2R in the presence of 0.7 nM of [$^3$H]CP55940 as high-affinity orthosteric CBRs radioligand. We screened all the compounds **C1-C12** at 100 nM on both CB1R and CB2R to test their CBR binding affinity (Fig. 2a and 2b). Regarding CB1R, most of the compounds (**C1, C2, C3, C5, C6, C8, C9, C11** and **C12**) resulted to be inactive at this
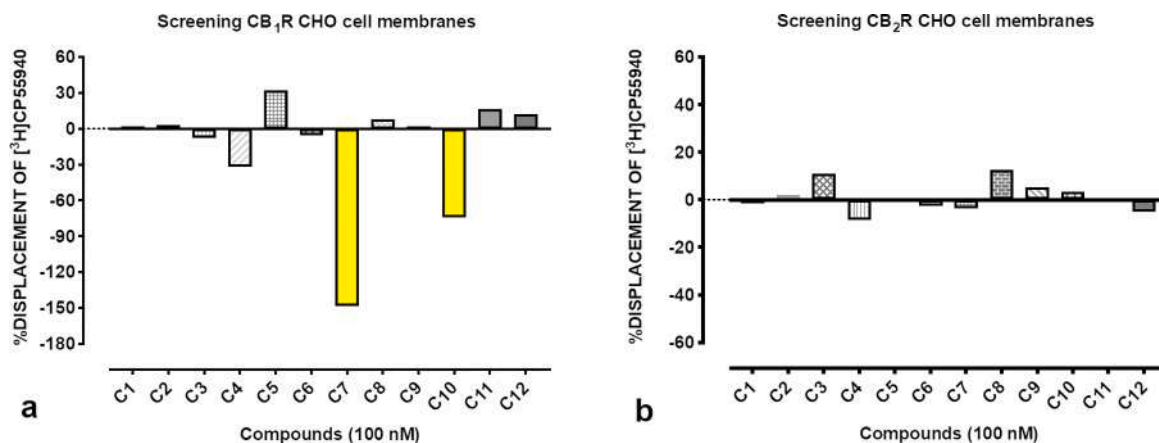
**Fig. 2.** a: Preliminary screening of compounds C1-C12 on CB1R. Yellow columns indicate compounds that significantly increase the binding of [³H]CP55940. b: Preliminary screening of compounds C1-C12 on CB2R. Data are mean with 95% confidence intervals of 3–6 independent experiments.
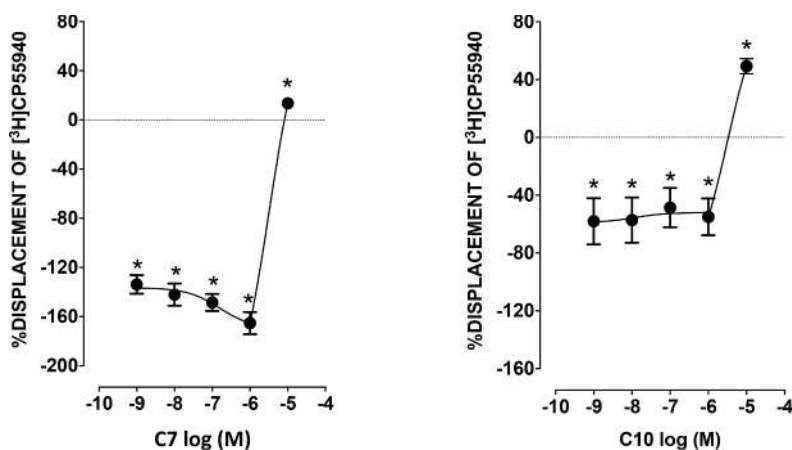


**Fig. 3.** Concentration-binding curves of **C7** and **C10**. Asterisks indicate mean values significantly different from zero (*$P < 0.05$) (one sample *t*-test). In the experiments $n = 6$.

concentration (100 nM). Nevertheless, rather unexpectedly, for compounds **C4, C10** and **C7** we did not detect displacement of the radioligand ([³H]CP55940) but increased binding to this receptor as indicated by negative values of the percentage of displacement in Fig. 2A.

Compounds **C7** and **C10** are the best enhancers inducing approximately a 150% and 70% increase in the binding of [³H]CP55940, respectively. Instead compound **C4** was a weak enhancer inducing only approximately 30% increase in the binding of radioligand (Fig. 2A).

Concerning CB2R, the results indicate that none of these compounds significantly displace or enhance the binding of the radioligand [³H]CP55940 (Fig. 2B).

Compounds **C7** and **C10**, that were the most effective enhancers at 100 nM on CB1R, have been tested at different concentrations to construct a dose-response binding curve (Fig. 3).

Derivative **C10** was found to enhance weakly the binding of [³H]CP55940, whereas compound **C7** strongly increased the binding of [³H]CP55940 at very low concentrations (Fig. 3) confirming its allosteric behavior.

Following this result we decided to continue to deepen the study of **C7**. It was tested at different concentrations to construct a dose-response binding curve (Fig. 3) showing to significantly enhance the binding of [³H]CP55940 up to $10^{-9}$ M. Then, since both original classes **A** and **B** have been tested for their functional activity using [³⁵S]GTPγS assays,
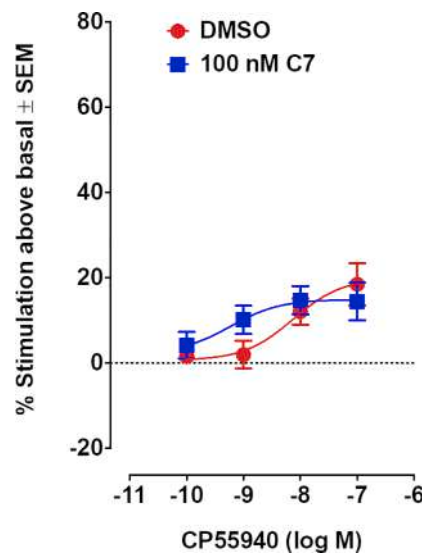


**Fig. 4.** CB2R [³⁵S]GTPγS assays performed with CP55940 and compound **C7** (un- paired *t*-test) ($n = 5$).

**C7** was tested in the same assay as well.

[$^{35}$S]GTPγS assays were carried out in the presence of [$^{35}$S]GTPγS (0.1 nM), GDP (30 μM), GTPγS (30 μM), with CHO cell membranes (1 mg/ml) overexpressing *h*CB1R. The effects of **C7** on the modulation of CB1R-mediated signaling were studied by measuring [$^{35}$S]GTPγS receptor binding (Fig. 4).

As shown in Fig. 4, CP55940-induced stimulation of [$^{35}$S]GTPγS receptor binding was not significantly altered by 100 nM **C7**. Our choice of a **C7** concentration of 100 nM for these experiments was influenced by the CB1R binding data. This result suggests that although this concentration of compound **C7** enhances the binding of the orthosteric ligand, [$^3$H]CP55940, to CB1R, this enhancement does not significantly affect the ability of CP55940 to activate CB1R through this specific signaling pathway.

On the basis of binding studies, despite results of [$^{35}$S]GTPγS assays, we decided to use a computational approach, to understand the specific interactions of **C7** and **C10** at the binding site, compared to the other compounds **C** which did not show an allosteric behavior. For this purpose, we analyzed both NAM and PAM binding sites, the first one detected through crystallographic studies, (Shao et al., 2019) the second one hypothesized on the basis of experimental evidences, as possible sites of interaction for our compounds **C**.

### 3.3. Computational studies

#### 3.3.1. Compounds selection

The computational study started with the selection of known allosteric modulators of CB1R which share with our **C** compounds a positive binding cooperativity with the orthosteric ligand CP55940. The hypothesis, developed thanks to the resolution of CP55940/ORG27569-bound CB1, (Shao et al., 2019) is that the allosteric ligand induces a conformational change of some aromatic residues (Phe273 and Phe155 for ORG27569-bound CB1). (Shao et al., 2019) This modification promotes a rotation of the extracellular half of TM2 which is responsible of an orthosteric binding site contraction, probably related to the potentiating effect on wild-type CB1 binding to [$^3$H]CP55940. (Shao et al., 2019) We can suppose, indeed, that our **C** compounds share the same binding site of a known allosteric ligand if, at least, the effect on the orthosteric agonist binding to CB1R is the same. Effects on potency or efficacy are much more complex to correlate in terms of binding site position. Since these effects are related to receptor activation and Gi protein binding, resulting in large changes in helix arrangement, it is hard to assume that NAM and PAM may share the same binding site.

Among NAMs, the organon compounds, like the crystallized ORG27569, and also the urea derivative PSNCBAM-1 (Fig. 5), are able to dose-dependently enhance [$^3$H]CP55940 binding. (Nguyen Li et al., 2017) So, we performed our study using ORG27569 and PSNCBAM-1 as reference NAMs, to compare our results for **C** compounds with them. Among PAMs, tropane derivatives like RTI-371 or JHW007 (Fig. 5) show a positive allosteric effect, displaying concentration-dependent increases in the E$_{max}$ of CP55940 activity, but at the moment we have no information about their effect on CP55940 binding. Regarding the recently reported small compounds ZCZ011 and GAT229, there is evidence they are able to increase the [$^3$H]CP55940 specific binding to CB1R acting as PAMs. (Ignatowska-Jankowska et al., 2015; Laprairie et al., 2017) For this reason, ZCZ011 and GAT229 were used as reference PAMs. However, RTI-371 and JHW007 were studied, to determine their location in CB1R.
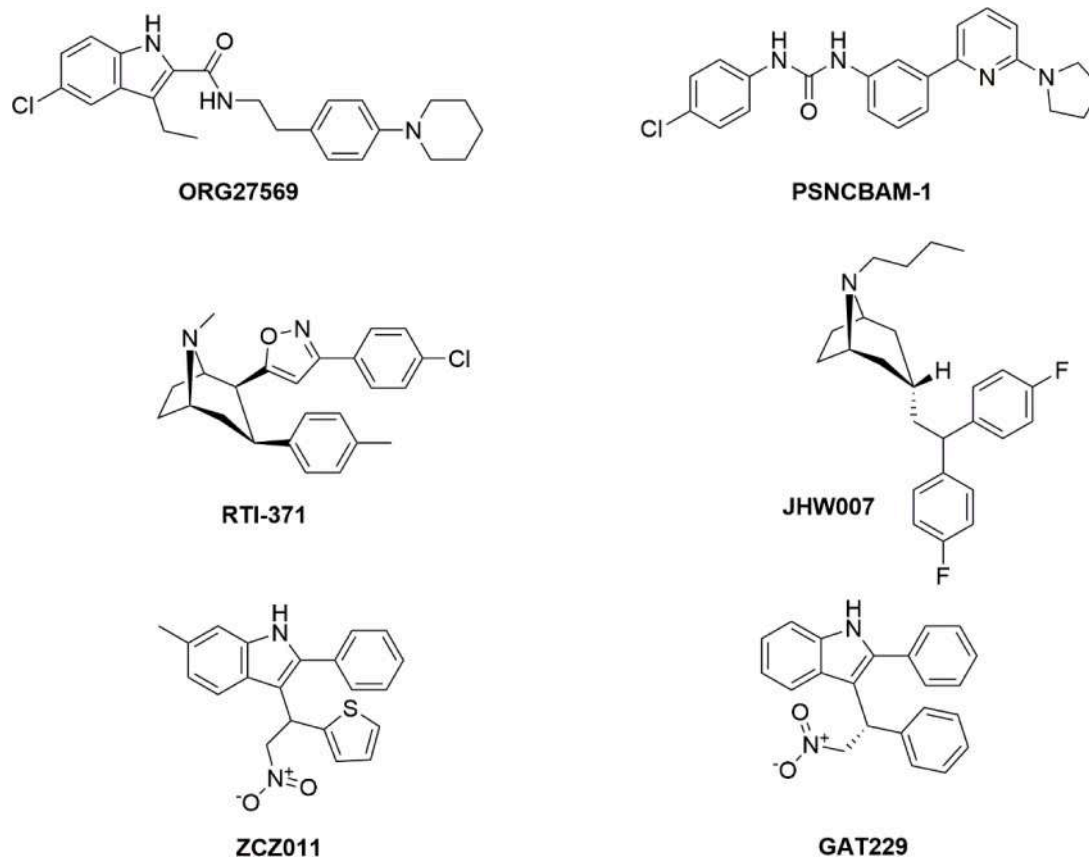


**Fig. 5.** Known CB1R allosteric modulators used as reference compounds in this study: ORG27569 and PSNCBAM-1 (NAMs), RTI-371, JHW007, ZCZ011 and GAT229 (PAMs).

**Table 2**

Flap score relative to H*C1= probes, the product of the H and aromatic MIF overlaps. In bold active compounds, in italic decoys, in normal text inactive compounds.

| Compound | H*C1= (score) |
| --- | --- |
| **ORG27569** | 0.59 |
| **PNSCBAM1** | 0.44 |
| *C7* | 0.41 |
| *C10* | 0.39 |
| C2 | 0.38 |
| RTI-371 | 0.37 |
| C12 | 0.37 |
| C11 | 0.36 |
| C4 | 0.36 |
| C6 | 0.36 |
| C9 | 0.36 |
| C5 | 0.35 |
| C1 | 0.35 |
| C8 | 0.34 |
| GAT229 | 0.34 |
| JHW007 | 0.32 |
| C3 | 0.32 |
| (R)-ZCZ011 | 0.29 |
| (S)-ZCZ011 | 0.27 |

**Table 3**

Flap score relative to DRY*C1= probes, the product of the lipophilic and aromatic MIF overlaps. In bold active compounds, in italic decoys, in normal text inactive compounds.

| Compound | DRY*C1= (score) |
| --- | --- |
| **ORG27569** | 0.40 |
| **PNSCBAM1** | 0.29 |
| *C7* | 0.27 |
| *C10* | 0.25 |
| RTI-371 | 0.24 |
| C11 | 0.23 |
| GAT229 | 0.22 |
| C1 | 0.22 |
| C9 | 0.22 |
| C5 | 0.22 |
| C4 | 0.22 |
| C6 | 0.21 |
| C12 | 0.21 |
| C2 | 0.20 |
| C8 | 0.20 |
| (R)-ZCZ011 | 0.19 |
| (S)-ZCZ011 | 0.16 |
| JHW007 | 0.16 |
| C3 | 0.15 |

**Table 4**

Flap score relative to N1*O probes, the product of the donor and acceptor MIF overlaps. In bold active compounds, in italic decoys, in normal text inactive compounds.

| Compound | N1*O (score) |
| --- | --- |
| **GAT229** | 0.99 |
| **(S)-ZCZ011** | 0.29 |
| **(R)-ZCZ011** | 0.26 |
| **RTI-371** | 0.16 |
| **JHW007** | 0.11 |
| C5 | 0.07 |
| C4 | 0.06 |
| ORG27569 | 0.06 |
| C1 | 0.06 |
| C2 | 0.05 |
| PSNCBAM1 | 0.05 |
| *C7* | 0.04 |
| C8 | 0.04 |
| C6 | 0.04 |
| C11 | 0.03 |
| C9 | 0.03 |
| *C10* | 0.03 |
| C12 | 0.02 |
| C3 | 0.01 |

JHW007 are the last ones.

The superposition of NAMs using the DRY*C= probe led to predict the alignment of the fluorophenyl tail of PSNCBAM-1 on the fluoroindole of ORG27569, superposing the aniline of PSNCBAM-1 on the piperidine of ORG27569. The screening through the H*C= probe, on the contrary, predicted a reversed alignment of PSNCBAM-1 on ORG27569, superposing the aniline of PSNCBAM-1 on the fluoroindole of ORG27569 (data not shown). Ranking of compounds is very similar, as well as the **C7** alignment. The cyclohexanol- of **C7** is aligned to the fluoroindole moiety of ORG27569, and the methoxyphenyl superposed with the piperidine (see Fig. S5a).

Conversely, FLAP superposition of our **C** compounds on GAT229 produced a screening model able to discriminate PAMs and NAMs using the combination O*N1 probes, and not DRY and/or C= probes, with an AUC of 1. The first hits of the screening are all known PAMs (Table 4). Ranking position of our **C** compounds is after NAMs PSNCBAM-1 and ORG27569: the features involved in the PAM activity are polar functional groups, and the ranking position of **C7** and **C10** is 10 and 15, respectively. The model alignment is reported in Fig. S5b: there is no particular correlation between the polar or aromatic groups of **C7** and PAMs. The ranking of **C7** and **C10** compared to NAM and PAM templates, and the chemical features involved, are the first evidence on our **C** compounds behavior that we can add to the structure-based study described later.

### 3.3.3. Structure based study: CB1 cavities identification

A preliminary analysis of the possible allosteric binding sites was performed through a blind docking in all the available CB1 receptor structures using the GOLD program, (Verdonk et al., 2003) and through a pocket search using FLAP. (Baroni et al., 2007) The two programs work using different methods, but results are in good agreement. GOLD calculated a list of hydrophobic fitting points in the binding site, which are used during the generation of trial docking solutions to map hydrophobic ligand atoms into favorable regions of the binding site. The FLAPsite pocket detection algorithm locates potential pockets in the protein using the DRY probe to identify hydrophobic regions. Neighboring grid points with similar indices above a certain threshold are combined into clusters, and then a morphological refinement through both erosion and dilation steps, limited by the protein surface, is applied. All available crystal structures are used, in all the activation states. In Fig. 6, one example for each activation state is reported.

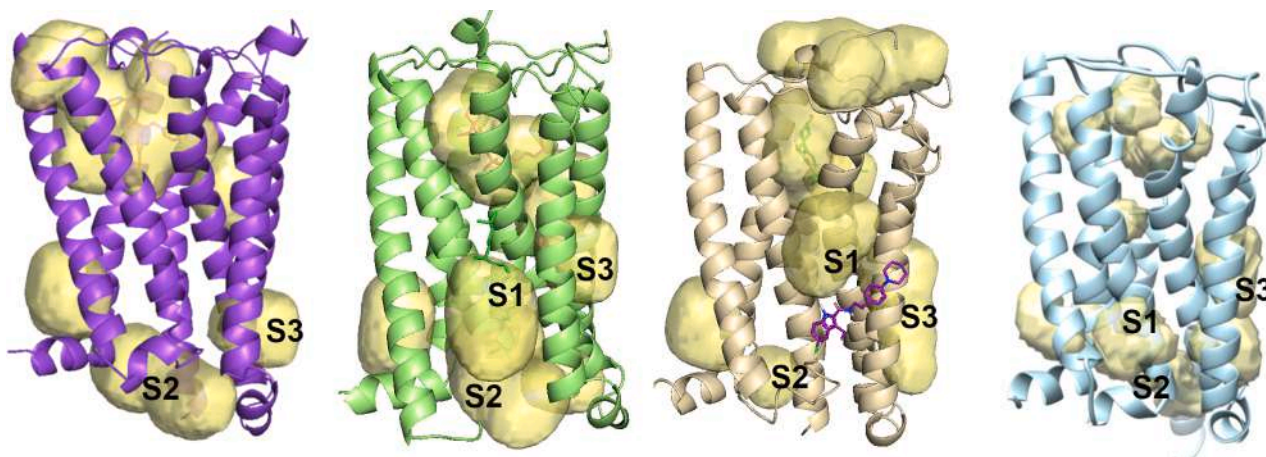GOLD detected three main possible allosteric sites: the ORG27569

### 3.3.2 Ligand based study

A FLAP (Cross et al., 2012; Cross et al., 2010) ligand based screening of **C** compounds was performed using ORG27569 as a NAM template and GAT229 as a PAM template. In this way we investigated if **C** compounds could have a better alignment on NAM or PAM templates, both experimentally related to an enhancement of wild-type CB1 binding to [³H]CP55940, but potentially involved in different mechanisms and/or different binding sites. The superposition of our **C** compounds on ORG27569 produced a screening model able to discriminate ORG27569 and PSNCBAM-1 with respect to ZCZ011, GAT229, RTI-371 and JHW007 using all the combinations of H, DRY, C= (aromatic) probes, with an AUC of 1. This is a predictable result, considering shape and chemical difference among NAM and PAM structures. As reported in Tables 2 and 3, both using H*C1= or DRY*C1= combinations, a mix of shape and aromatic features the first, and of lipophilic and aromatic features the second, our NAM template ORG27569, PSNCBAM-1, and the new derivatives **C7** and **C10** are the first 4 ranked compounds. ZCZ011 (built in both enantiomeric forms, being a racemate) and

**Fig. 6.** Summary of receptor cavities predicted by Flap program in 5UO9 structure (Shao et al., 2016) (inactive form), 5XRA[222] (agonist-bound form), 6KQI (Shao et al., 2019) (agonist and NAM bound complex) and 6BN4[26] (agonist and Gi-bound complex).

binding site S1 (which is the same site as cholesterol in 5XRA complex (Hua et al., 2016)), the site of interaction with Gi protein (S2), and a third site corresponding to the cholesterol binding site in 6N4B complex (Kumar et al., 2019) (S3). FLAP, in addition to some secondary pockets too small for docking ligands, detected the S1, S2 and S3 pockets as reported in Fig. 6 (different in size and distribution among different activation states), and ancillary pockets at the extracellular hindrance of the orthosteric ligand, in different parts of the loop region. No one of these pockets corresponds with the possible CB1R binding region identified for GAT229 using a very different method, the force-biased MMC simulated annealing. (Hurst et al., 2019)

Docking in the S2 pocket is not reliable, because it is the binding region of Gi protein, so it was not considered for successive studies. The S3 pocket was analyzed, in particular regarding i) the presence of aromatic residues, usually involved in the activation mechanism, ii) the presence of residues already subjected to mutagenesis studies, and iii) the relative position of the S3 helices TM3, TM4 and TM5 in different activation states. The cholesterol site is very large, and presents two aromatic residues in crucial position, Phe208 and Phe289, showing different conformation among different CB1 crystal structures (Fig. S6).

The opened conformation of Phe289 in the antagonist-bound form matches with a peculiar disposition of Tyr294, which clashes with TM3 in the active state. In the agonist-bound CB1 structures, Tyr294 is positioned towards Tyr397 of TM7, engaging in the Gi-bound state a strong hydrogen bond. The relationship between Phe289 conformation

and Tyr294 disposition is not clear, but surely it is related to a TM5 rearrangement switching from inactive to active form, which allows Tyr294-Tyr397 interaction stabilizing the G-coupling active state. This is in agreement with some previous molecular dynamics results: the cluster formed by the aromatic residues around Y215 (Fig. 7), including Phe208, Phe289, Tyr292, and Tyr296, appears to be important for stabilizing TM3/TM5 association at the intracellular region. Shim (2009) Analyzing the mutation results, no data about the surface residues of TM3,4 and 5 is reported, but Leu207Ala and Thr210Ile mutant, near Tyr397, influences constitutive activity of CB1R (not shown). (Al-Zoubi et al., 2019) In particular, it's interesting the role of the conserved DRY motif, which stabilizes the inactive state of the receptor by forming an ionic interaction between Asp213 and Arg214 (Fig. 7) in the inactive state, being Asp213 accessible from the S3 site surface. Also Phe155, which is involved in allosteric modulation, shares the same site as Asp213 and it is accessible from the S3 site surface, nevertheless it is part of TM2.

Regarding the relative positions of TM3, TM4 and TM5 in the S3 region, there is an evident shift of TM3 and TM5 during the activation, which led to a reduction in TM3-TM5 distance and an increment of TM3-TM4 distance in the intracellular half of TM tract. This causes an enlargement of the region of S3 near the CLR1 site in 6N4B crystal structure (Fig. S7).

Finally, this region corresponds with the binding site of AgoPAM AP8 in the GPR40 x-Ray structure. (Lu et al., 2017) For all these reasons, the
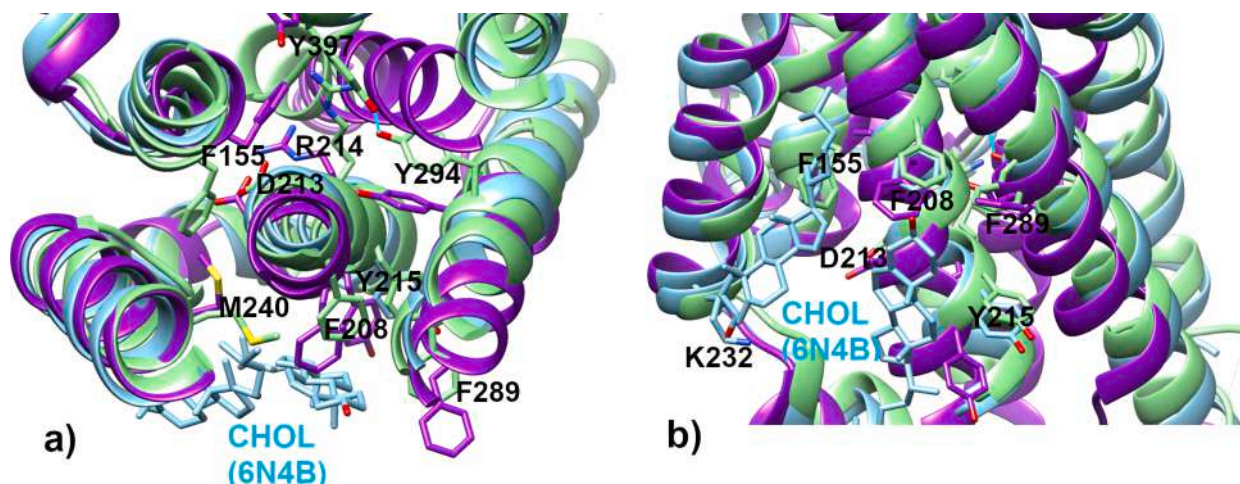


**Fig. 7.** a) top view and b) front view of S3 cholesterol binding site in superposed 6N4B (agonist and Gi-bound, cyan); 5XRA (agonist bound complex, green) and 5UO9 (antagonist bound, purple). Key residues are visualized.

region S3 was considered as a possible binding site for PAMs.

### 3.3.4. Docking in pockets S1 and S3

Selected NAMs (ORG27569 and PSNCBAM-1) and PAMs (ZCZ011 and GAT229, RTI-371 and JHW007) are used for exploring S1 and S3 pockets in different states of activation of CB1R. Our aim was to identify, within cavities, the most plausible one for binding NAMs and PAMs. It has been proposed that the negative influence of NAMs on the orthosteric agonist efficacy was related to the stabilization of an intermediate conformation, in which the orthosteric binding site mimics the active state, but TM6 movement is hindered by the interaction of crystallized ORG27569 with Phe237 (and indirectly with Phe155) in its inactive conformation. (Shao et al., 2019) This aromatic arrangement, in a region about 20 Å far from the agonist, disfavors the repacking involved in the activation of the receptor. We can hypothesize a similar mechanism for the positive influence of PAMs on the orthosteric agonist efficacy, supposing that the PAM binding cavity is the one which can mediate a hindrance of the repacking involved in the active-inactive state transition.

#### 3.3.4.1. Docking in S1 cavity.
Docking in the experimental binding site of ORG27569 is, obviously, the most reliable for NAMs. A good docking protocol for obtaining the right redocking of the ligand was achieved after many attempts, resulting in two possible orientations with similar scores, one showing a RMSD between experimental and docking pose of 1.3 Å (Fig. 8a, flaxen colored), and an alternative reversed pose. PSNCBAM-1 (Fig. 8a, brown colored) occupies the same region with an analogue pose. Also for this ligand, GOLD program suggested a second reversed pose with similar score, coherently with the Flap ligand based study. Both ligands engage no polar interactions with receptor; in particular, it is not clear the role of the aniline nitrogen, which seems not involved in hydrogen bonds with Thr242. This nitrogen is not present in all NAMs, or it is not at the same distance from the indole-carboxamide moiety. (Morales et al., 2016) The key interaction seems to be related to the conserved Trp241 and the aromatic core of these ligands; this is enhanced by the amide or urea moieties which extends, especially in PSNCBAM-1, the electronic delocalization. The comparison among the NAM poses and the experimental cholesterol binding mode (PDB code 5XRA, yellow in Fig. 8a), shows a similar interaction of the rigid core of sterol, the diphenylurea of PSNCBAM-1 and the indole-carboxamide of ORG27569 with the region enclosed by His154, Phe237 and Trp241. These rigid blocks preclude the aromatic rearrangement of the binding site residues, and guarantee a strong $\pi-\pi$ interaction with Trp241. Our **C** compounds have different shape and size than NAMs and PAMs, but they fit the experimental binding site of ORG27569, in some cases hindering Phe237 region (see Fig. 8b-e). The pose of our **C** compounds is analogue to the superposition of the experimental pose of cholesterol (yellow colored in Fig. 8a) and the aromatic tail of ORG27569 (flaxen colored in Fig. 8a), which is aligned in the crystal structure with the steroid position 18. In particular, compounds bearing a methoxy substituent on the phenyl tail (**C4**, **C10**, **C1** and **C7**, Fig. 8b), insert more deeply in the receptor due to the hydrogen bond with Thr214. **C7** (brown colored), thanks to the intramolecular hydrogen bond between the amide nitrogen and the methoxyl moiety on the central phenyl, directs the amide carbonyl to Cys238. Furthermore, the intramolecular H-bond increases the rigidity and coplanarity of the ligand, allowing a better $\pi-\pi$ interaction with Trp241. All these interactions pull **C7** in the deeper region of Phe237, allowing a further interaction with His154. The **C7** hydroxyl position is analogue to the hydroxyl position of cholesterol in 5XRA crystal structure, where it interacts with an oleic acid molecule (not shown in Fig. 7). A progressive reduction in the interaction strength and in the binding depth is observed from **C7** to: 1) **C10** (light blue colored, Fig. 8b), which lacks of the methoxyl moiety on the central phenyl, indirectly responsible of the interaction with Cys238 as described before, and moves about 1 Å upper than His154 and Phe237; 2) **C4**

(purple colored, Fig. 8d), with its bulkiest and distorted cycloheptane, without any polar interaction with His154; and 3) **C1** (green colored, Fig. 8d), in which the bulkiest and distorted cycloheptane disfavors the intramolecular hydrogen bond between the methoxyl moiety on the central phenyl and the amide nitrogen. For this reason, the ligand moves above for avoiding the clash of the methoxyl moiety with Leu165. All other **C** modifications, which lose the possibility to interact with Thr214, are detrimental for the insertion in the key aromatic region of the S1 cavity: **C8** and **C9** (Fig. 8c: coral and green colored, respectively), despite the presence of the methoxyl moiety on the central phenyl, cannot bind in the same conformation of **C7**, engaging only the hydrogen bond between the cyclohexanol hydroxyl and Cys238. In the same way lie **C11** and **C12** (Fig. 8d: pink and green colored, respectively) with respect to **C10**, while **C5**, **C6**, **C3** and **C2** (Fig. 8e: yellow, green, dark, and light gray colored, respectively), losing the only possible interaction engaged by **C4** through its methoxy substituent with Thr214, cannot engage any polar interaction.

Docking of PAMs was performed in S1 cavity of the CB1R activated form (pdb code 6N4B), (Kumar et al., 2019) coherently with their activity. For JHW007, GOLD program could not produce any pose in this binding site. For GAT229, ZCZ011 and RTI-371 similar binding modes were predicted: all ligands engage interactions (Fig. 8f) with Arg148, through nitro group and oxazole ring respectively, but no rationalization about the roles of indole NH and tropane amine was detected. Furthermore, the position of the phenyl bonded to indole of GAT229 and ZCZ011, which is surrounded by aliphatic residues, cannot justify the decrease of potency if it is substituted with a cyclohexyl group. (Tseng et al., 2019) The key residue Phe237 is free to move, despite the binding to these PAMs, and the Arg148 region appears to be unaffected by the active-inactive form shift of CB1R. For these reasons, docking of our selected PAMs in this region, previously reported as possible binding region for ago-PAM GAT228, (Garai et al., 2020) seems to be not reliable for pure PAMs.

#### 3.3.4.2. Docking in S3 cavity.
Docking in the S3 cavity has been performed for searching an alternative possible binding mode for PAMs, coherent with biological data and with a plausible mechanism of positive modulation of the receptor activation. Results obtained from docking of PAMs in the S1 cavity, in fact, are not able to rationalize their properties.

GOLD program suggests for ZCZ011 and GAT229 the same pose in S3 cavity of 6N4B (see Fig. 9a), in the intracellular region, engaging a polar interaction with Lys232 *via* nitro group, a strong T-shaped aromatic interaction with Phe208, and a displaced interaction with Phe155, due to the phenyl insertion in the inner cavity. In both cases the indole NH seems to have no particular role. Experimentally, N-methyl and N-phenyl analogs are found less active or inactive, but we don't know if this is due to steric or electronic factors, lacking data on the indene derivative. Docking of ZCZ011 and GAT229 in S3 precludes the possibility to insert methyl or other substituent on indole -NH for steric factors, in agreement with a loss in potency for these analogs. Experimental replacement of nitro group of GAT229 with amine or $-CF_3$[38] reduced potency and efficacy: these data support that the $-NO_2$ group is involved in a strong hydrogen bond. All phenyls are important for allosteric activity; in particular, the one's bonded to indole, if substituted with a cyclohexyl group, preserves a slight potency, but its substitution with H leads to inactivity, and also the lack of benzene ring of indole leads to a dramatic drop in CB1R PAM activity. The role of the indole of ZCZ011 or GAT229 in the stabilization of the activated conformation of the receptor, seems to be related to its interaction with Phe155, which in the inactive form lies on the other side of TM2 due to a side chain rotation of about 180°, and in activated conformation displaced the key residue Phe237. The interaction between the phenyl adjacent to indole and Phe208 could have a role in stabilizing the position of TM3 in the activated conformation, precluding its shift towards
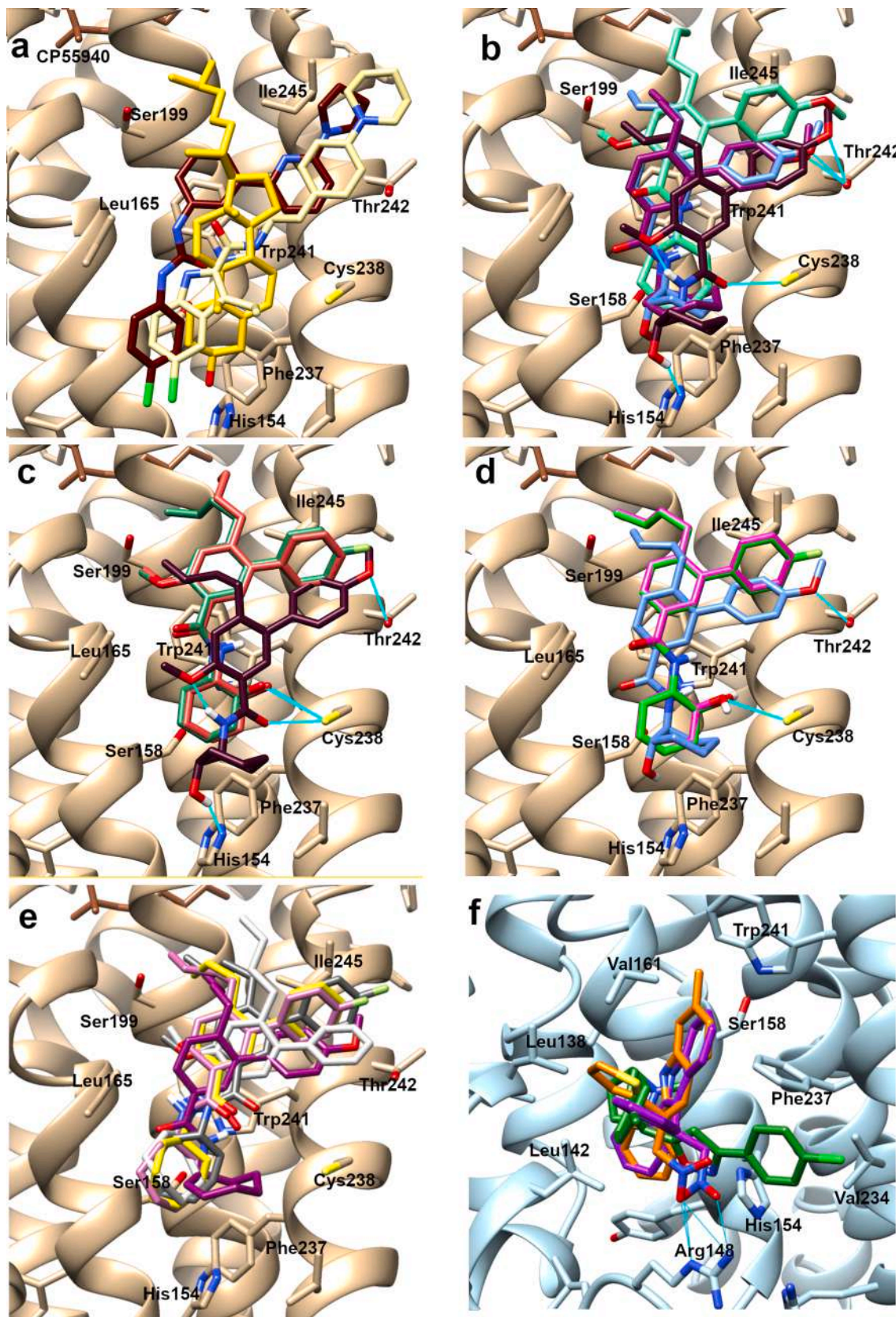
**Fig. 8.** Docking results in 6KQI structure (agonist and NAM bound complex). a) PSNCBAM-1 (brown colored) aligned with experimental pose of cholesterol (yellow) and ORG27569 (flaxen); b) C4 (purple), C10 (light blue), C1 (green) and C7 (dark brown); c) C8 (coral) and C9 (green) compared to C7 (dark brown); d) C11 (pink) and C12 (green) compared to C10 (light blue); e) C5 (yellow), C6 (green), C3 (dark gray) and C2 (light gray) compared to C4 (purple); f) ZCZ011 (purple), GAT229 (magenta) and RTI-371 (green).
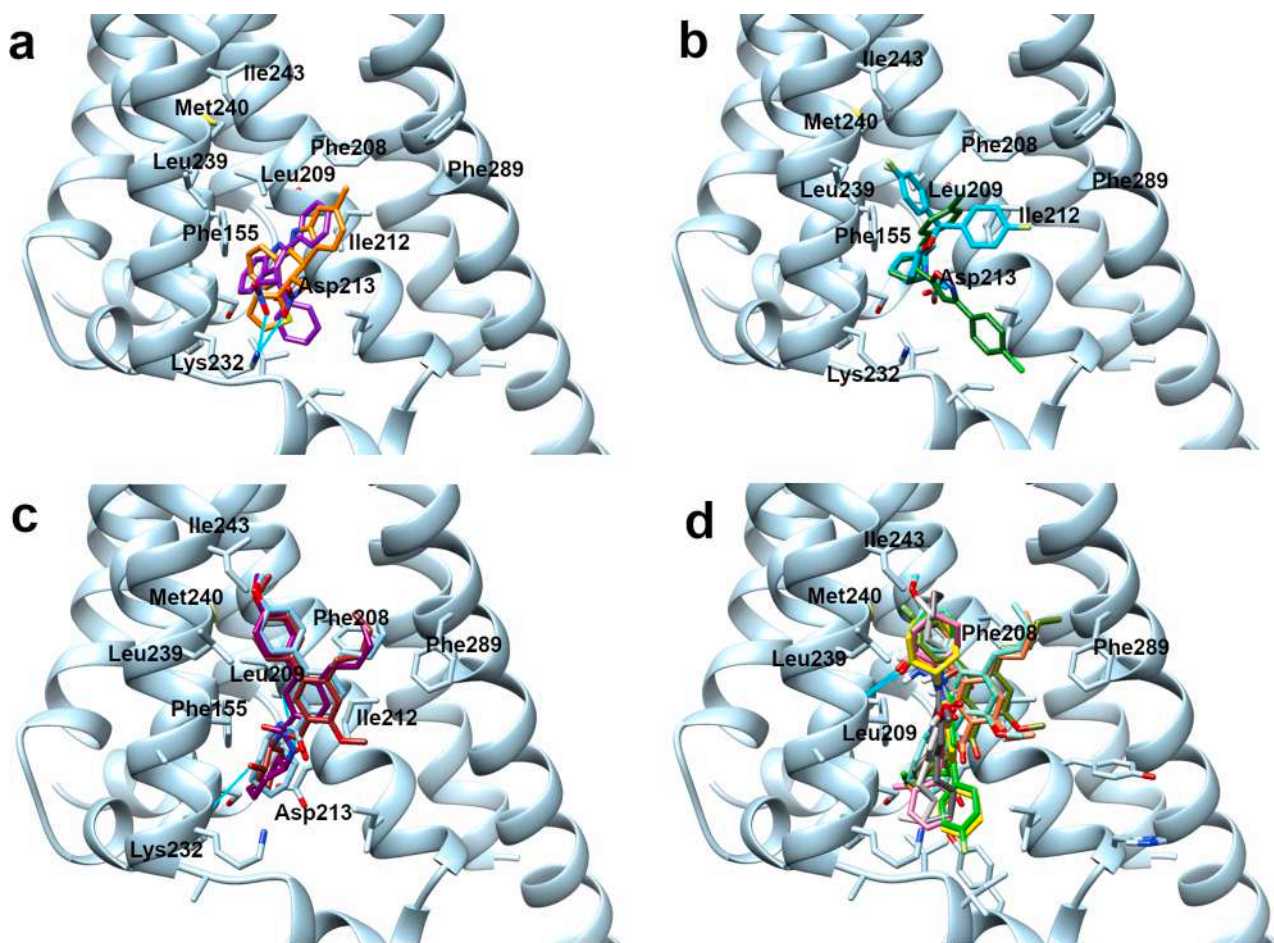
**Fig. 9.** Docking results in 6N4B structure (agonist and Gi-bound complex). a) ZCZ011 (purple) and GAT229 (magenta); b) RTI-371 (green) and JHW007 (cyan); c) C4 (purple), C10 (light blue) and C7 (brown); d) C5 (yellow), C6 (green), C11 (pink), C12 (green), C1 (light green), C8 (coral), C3 (dark gray), C9 (dark green) and C2 (light gray).

TM4 during the inactivation.

RTI-371 and JHW007 share the pose of tropane ring (see Fig. 9b), but their aromatic ramifications are divergent. The protonated moiety, as the indole of ZCZ011 or GAT229, is inserted in the inner part of the cavity where Asp213 directs its carboxylic group. This residue is part of the DRY motif, (Al-Zoubi et al., 2019) crucial for the inactivation: it stabilizes the inactive state of the receptor by forming an interaction with Arg214, and this interaction is broken upon activation of the receptor. The interaction of Asp213 with the protonated tropane could preclude its interaction with Arg214, disfavoring the transition to the inactive state. One of the aromatic rings of JHW007 interacts with Phe208, the other one with the aliphatic Leu239 and Ile243. The aromatic tails of RTI-371 are assessed in a different way with respect to JHW007, due to the polar interaction between the oxazole ring and Lys232. All these compounds share i) a cholesterol binding site, which is strategic for the activation-inactivation mechanism: as reported before, it is close to the activation switch, suggesting that CLR may impair the affinity of CB1 agonists indirectly by modulation of receptor activation; (Jakubík and El-Fakahany, 1953) ii) a crucial aromatic interaction with Phe208, which is not conserved in CB2, then could be a selective interaction; and iii) the presence of a key polar interaction, in agreement with the FLAP ligand-based results, which showed a good classification of actives and inactives using the combination of N1*O probes.

Our **C** compounds insert in S3 cavity occupying about the same region; the three active compounds (Fig. 9c: **C7, C10** and **C4**, brown, light blue, and purple colored, respectively) are not able to engage polar interactions; they direct the cyclohexyl moiety towards Phe155, the

aliphatic chain towards Phe208, losing the strong aromatic interactions previously described for PAMs. The methoxyl moiety seems to have no particular role, nevertheless biological results suggested a clear relationship between this group and activity. All other **C** compounds, reported in Fig. 9d, which have no effect on the agonist binding, have docking poses superposed to the last described (compounds **C1, C8** and **C9**, light green, coral, dark green colored, respectively), or up-down reversed (**C5, C11** and **C12**, yellow, purple, green colored, respectively), which allow a hydrogen bond with the backbone of Ala236. All these poses cannot rationalize a potential positive allosteric modulation related to the specific ability of **C7** or **C10**, within the **C** series, to potentiate CB1 binding to [$^3$H]CP55940.

The same docking, performed in the 6KQI structure, does not give poses in the same region of the S3 cavity, which is less accessible in the inactive form of the receptor.

Definitively, S3 cavity was confirmed by docking as a possible binding site for PAMs, since it is coherent with experimental information derived from mutagenesis studies and with structure-activity relationships of known PAMs. This cavity is the experimental binding site in the CB1R activated form for cholesterol, which is proposed to indirectly modulate the receptor activation. (Jakubík and El-Fakahany, 1953) This pocket, proposed and analyzed in this study for the first time, corresponds also with the experimental binding site of AgoPAM AP8 in the GPR40 crystallographic structure. (Lu et al., 2017)

## 4. Conclusion

This work provided additional information about the key groups involved in the interaction with both CBRs binding site. Considering the three CB1R binding enhancers **C4**, **C10** and **C7**, the R$_2$ substituent *trans*-2-hydroxycyclohexyl seems the most promising to have activity on CB1R. Moreover, all the 3 compounds present a –OCH$_3$ as R$_1$ substituent in phenyl group. The shift of the of the *n*-butyl substituent from position 5 to 6 leads to compounds which bind with high selectivity CB1R in agreement with the known compounds **A**. Furthermore, the presence of a small substituent at R$_3$ position seems to be well tolerated. From a pharmacological point of view, **C7** needs to be furtherly studied to clarify its nature. The fact that **C7** does not alter the CP55940-induced stimulation of [$^{35}$S]GTPγS receptor binding, might mean either it is a neutral allosteric modulator able to increase the binding without affecting the activity of CP55940, or that it selectively modulates different signaling pathways (biased signaling). For this reason, **C7** will be tested on other signaling pathways using ERK, cAMP or β-arrestin assays to verify its biased properties. Moreover, in case it activates at least one of these signaling pathways, **C7** will be also tested alone in the absence of a CB1R agonist, to verify if it is able to activate that specific signaling pathway independently demonstrating in this way a pure allosteric behavior.

At the moment, we can draw some conclusions on this topic, thanks to our computational study. Docking of our **C** compounds performed in the crystallographic site of ORG27569, a known NAM for CB1R, and in a hypothetical experimentally-driven binding site for PAMs, highlighted in the NAM site a different behavior of **C4**, **C10** and **C7** with respect to other **C** compounds. Furthermore, in this binding site, **C10** and, in particular, **C7** engage strong interactions with experimental key residues for allosteric modulation, while in the PAM binding site no strategic interaction is detected. Concluding, in this work we highlight that the combination of the pharmacophoric portions of two different classes of compounds **A** and **B** selective antagonists on CB1R or CB2R respectively, unexpectedly lead to a new class of compounds **C** with a totally different functional activity which has still to be demonstrated. A computational study on the three-dimensional structures of agonist/ORG27569-bound and agonist/Gi-bound form of CB1R indicates for these compounds a preferred interaction with the binding site for NAMs and also a possible location for the binding of PAMs was suggested

## Acknowledgement

## Supplementary materials

Supplementary material associated with this article can be found, in the online version, at doi:10.1016/j.ejps.2021.106088.

## References

Lu, H.-C., Mackie, K., 2016. An introduction to the endogenous cannabinoid system. Biol. Psychiatry 79 (7), 516–525. https://doi.org/10.1016/j.biopsych.2015.07.028.

Hu, S.S.-J., Mackie, K., 2015. Distribution of the endocannabinoid system in the central nervous system. In *Endocannabinoids*. In: Pertwee, R.G. (Ed.), Handbook of Experimental Pharmacology, 231. Springer International Publishing, Cham, pp. 59–93. https://doi.org/10.1007/978-3-319-20825-1_3.

Pertwee, R.G., Howlett, A.C., Abood, M.E., Alexander, S.P.H., Di Marzo, V., Elphick, M. R., Greasley, P.J., Hansen, H.S., Kunos, G., Mackie, K., Mechoulam, R., Ross, R.A., 2010. International union of basic and clinical pharmacology. LXXIX. Cannabinoid receptors and their ligands: beyond CB$_1$ and CB$_2$. Pharmacol Rev 62 (4), 588–631. https://doi.org/10.1124/pr.110.003004.

Nagappan, A., Shin, J., Jung, M.H., 2019. Role of cannabinoid receptor type 1 in insulin resistance and its biological implications. IJMS 20 (9), 2109. https://doi.org/10.3390/ijms20092109.

Lipina, C., Vaanholt, L.M., Davidova, A., Mitchell, S.E., Storey-Gordon, E., Hambly, C., Irving, A.J., Speakman, J.R., Hundal, H.S., 2016. CB1 receptor blockade counters age-induced insulin resistance and metabolic dysfunction. Aging Cell 15 (2), 325–335. https://doi.org/10.1111/acel.12438.

Muller, T., Demizieux, L., Troy-Fioramonti, S., Gresti, J., Pais de Barros, J.-.P., Berger, H., Vergès, B., Degrace, P., 2017. Overactivation of the endocannabinoid system alters the antilipolytic action of insulin in mouse adipose tissue. Am. J. Physiol. Endocrinol. Metabol. 313 (1), E26–E36. https://doi.org/10.1152/ajpendo.00374.2016.

Rubio, M.A., Gargallo, M., Isabel Millán, A., Moreno, B., 2007. Drugs in the treatment of obesity: sibutramine, orlistat and rimonabant. Public Health Nutr. 10 (10A), 1200–1205. https://doi.org/10.1017/S1368980007000717.

Samat, A., Tomlinson, B., Taheri, S., Thomas, G., 2008. Rimonabant for the Treatment of Obesity. PRC 3 (3), 187–193. https://doi.org/10.2174/157489008786264014.

Moreira, F.A., Grieb, M., Lutz, B., 2009. Central side-effects of therapies based on CB1 cannabinoid receptor agonists and antagonists: focus on anxiety and depression. Best Pract. Res. Clin. Endocrinol. Metabol. 23 (1), 133–144. https://doi.org/10.1016/j.beem.2008.09.003.

Blasio, A., Iemolo, A., Sabino, V., Petrosino, S., Steardo, L., Rice, K.C., Orlando, P., Iannotti, F.A., Di Marzo, V., Zorrilla, E.P., Cottone, P., 2013. Rimonabant precipitates anxiety in rats withdrawn from palatable food: role of the Central Amygdala. Neuropsychopharmacol 38 (12), 2498–2507. https://doi.org/10.1038/npp.2013.153.

Nogueiras, R., Veyrat-Durebex, C., Suchanek, P.M., Klein, M., Tschop, J., Caldwell, C., Woods, S.C., Wittmann, G., Watanabe, M., Liposits, Z., Fekete, C., Reizes, O., Rohner-Jeanrenaud, F., Tschop, M.H., 2008. Peripheral, but not central, CB1 antagonism provides food intake-independent metabolic benefits in diet-induced obese rats. Diabetes 57 (11), 2977–2991. https://doi.org/10.2337/db08-0161.

Cluny, N., Vemuri, V., Chambers, A., Limebeer, C., Bedard, H., Wood, J., Lutz, B., Zimmer, A., Parker, L., Makriyannis, A., Sharkey, K., 2010. A novel peripherally restricted cannabinoid receptor antagonist, AM6545, reduces food intake and body weight, but does not cause malaise, in rodents: peripheral CB antagonist reduces food intake. Br. J. Pharmacol. 161 (3), 629–642. https://doi.org/10.1111/j.1476-5381.2010.00908.x.

Han, J.H., Shin, H., Park, J.-.Y., Rho, J.G., Son, D.H., Kim, K.W., Seong, J.K., Yoon, S.-.H., Kim, W., 2019. A novel peripheral cannabinoid 1 receptor antagonist, AJ5012, improves metabolic outcomes and suppresses adipose tissue inflammation in obese mice. FASEB J. 33 (3), 4314–4326. https://doi.org/10.1096/fj.201801152RR.

Röver, S., Andjelkovic, M., Bénardeau, A., Chaput, E., Guba, W., Hebeisen, P., Mohr, S., Nettekoven, M., Obst, U., Richter, W.F., Ullmer, C., Waldmeier, P., Wright, M.B., 2013. 6-Alkoxy-5-Aryl-3-Pyridinecarboxamides, a new series of bioavailable cannabinoid receptor type 1 (CB1) antagonists including peripherally selective compounds. J. Med. Chem. 56 (24), 9874–9896. https://doi.org/10.1021/jm4010708.

Bertini, S., Parkkari, T., Savinainen, J.R., Arena, C., Saccomanni, G., Saguto, S., Ligresti, A., Allarà, M., Bruno, A., Marinelli, L., Di Marzo, V., Novellino, E., Manera, C., Macchia, M., 2015. Synthesis, biological activity and molecular modeling of new biphenylic carboxamides as potent and selective CB2 receptor ligands. Eur J Med Chem 90, 526–536. https://doi.org/10.1016/j.ejmech.2014.11.066.

Gentry, P.R., Sexton, P.M., Christopoulos, A., 2015. Novel allosteric modulators of G protein-coupled receptors. J. Biol. Chem. 290 (32), 19478–19488. https://doi.org/10.1074/jbc.R115.662759.

Alaverdashvili, M., Laprairie, R.B., 2018. The future of type 1 cannabinoid receptor allosteric ligands. Drug Metab. Rev. 50 (1), 14–25. https://doi.org/10.1080/03602532.2018.1428341.

Shao, Z., Yan, W., Chapman, K., Ramesh, K., Ferrell, A.J., Yin, J., Wang, X., Xu, Q., Rosenbaum, D.M., 2019. Structure of an allosteric modulator bound to the CB1 cannabinoid receptor. Nat. Chem. Biol. 15 (12), 1199–1205. https://doi.org/10.1038/s41589-019-0387-2.

Cross, S., Baroni, M., Goracci, L., Cruciani, G., 2012. GRID-based three-dimensional pharmacophores I: fLAPpharm, a novel approach for pharmacophore elucidation. J Chem Inf Model 52 (10), 2587–2598. https://doi.org/10.1021/ci300153d.

Cross, S., Baroni, M., Carosati, E., Benedetti, P., Clementi, S., 2010. FLAP: GRID molecular interaction fields in virtual screening. validation using the DUD data set. J Chem Inf Model 50 (8), 1442–1450. https://doi.org/10.1021/ci100221g.

Berman, H.M., 2000. The Protein data bank. Nucleic. Acids. Res. 28 (1), 235–242. https://doi.org/10.1093/nar/28.1.235.

Hua, T.; Vemuri, K.; Pu, M.; Qu, L.; Han, G.W.; Wu, Y.; Zhao, S.; Shui, W.; Li, S.; Korde, A.; Laprairie, R.B.; Stahl, E.L.; Ho, J.-.H.; Zvonok, N.; Zhou, H.; Kufareva, I.; Wu, B.; Zhao, Q.; Hanson, M.A.; Bohn, L.M.; Makriyannis, A.; Stevens, R.C.; Liu, Z.-.J. Crystal structure of the human cannabinoid receptor CB1. *Cell* 2016, 167 (3), 750–762. e14. https://doi.org/10.1016/j.cell.2016.10.004.

Shao, Z., Yin, J., Chapman, K., Grzemska, M., Clark, L., Wang, J., Rosenbaum, D.M., 2016. High-resolution crystal structure of the human CB1 cannabinoid receptor. Nature 540 (7634), 602–606. https://doi.org/10.1038/nature20613.

Hua, T.; Vemuri, K.; Nikas, S.P.; Laprairie, R.B.; Wu, Y.; Qu, L.; Pu, M.; Korde, A.; Jiang, S.; Ho, J.-.H.; Han, G.W.; Ding, K.; Li, X.; Liu, H.; Hanson, M.A.; Zhao, S.; Bohn, L.M.; Makriyannis, A.; Stevens, R.C.; Liu, Z.-.J. Crystal structures of agonist-bound human cannabinoid receptor CB1. *Nature* 2017, 547 (7664), 468–471. https://doi.org/10.1038/nature23272.

Hua, T.; Li, X.; Wu, L.; Iliopoulos-Tsoutsouvas, C.; Wang, Y.; Wu, M.; Shen, L.; Brust, C.A.; Nikas, S.P.; Song, F.; Song, X.; Yuan, S.; Sun, Q.; Wu, Y.; Jiang, S.; Grim, T.W.;

Benchama, O.; Stahl, E.L.; Zvonok, N.; Zhao, S.; Bohn, L.M.; Makriyannis, A.; Liu, Z.-. J. Activation and signaling mechanism revealed by cannabinoid receptor-Gi complex structures. *Cell* 2020, 180 (4), 655–665. e18. https://doi.org/10.1016/j. cell.2020.01.008.

Krishna Kumar, K., Shalev-Benami, M., Robertson, M.J., Hu, H., Banister, S.D., Hollingsworth, S.A., Latorraca, N.R., Kato, H.E., Hilger, D., Maeda, S., Weis, W.I., Farrens, D.L., Dror, R.O., Malhotra, S.V., Kobilka, B.K., Skiniotis, G, 2019. Structure of a signaling cannabinoid receptor-G protein complex. Cell 176 (3), 448–458. https://doi.org/10.1016/j.cell.2018.11.040 e12.

Schrödinger Inc. Macromodel. Portland, OR 2009.

Al-Zoubi, R., Morales, P., Reggio, P.H., 2019. Structural insights into CB1 receptor biased signaling. Int J Mol Sci 20 (8), 1837. https://doi.org/10.3390/ijms20081837.

Baroni, M., Cruciani, G., Sciabola, S., Perruccio, F., Mason, J.S., 2007. A common reference framework for analyzing/comparing proteins and ligands. fingerprints for ligands and proteins (FLAP): theory and application. J. Chem. Inf. Model 47 (2), 279–294. https://doi.org/10.1021/ci600253e.

Verdonk, M.L., Cole, J.C., Hartshorn, M.J., Murray, C.W., Taylor, R.D., 2003. Improved protein-ligand docking using GOLD. Proteins Struct. Funct. Bioinf. 52 (4), 609–623. https://doi.org/10.1002/prot.10465.

Nguyen Li, T.J.-X., Thomas, B.F., Wiley, J.L., Kenakin, T.P., Zhang, Y., 2017. Allosteric modulation: an alternate approach targeting the cannabinoid CB1 receptor. Med. Res. Rev. 37 (3), 441–474. https://doi.org/10.1002/med.21418.

Ignatowska-Jankowska, B.M., Baillie, G.L., Kinsey, S., Crowe, M., Ghosh, S., Owens, R.A., Damaj, I.M., Poklis, J., Wiley, J.L., Zanda, M., Zanato, C., Greig, I.R., Lichtman, A.H., Ross, R.A., 2015. A cannabinoid CB1 receptor-positive allosteric modulator reduces neuropathic pain in the mouse with no psychoactive effects. Neuropsychopharmacology 40 (13), 2948–2959. https://doi.org/10.1038/ npp.2015.148.

Laprairie, R.B., Kulkarni, P.M., Deschamps, J.R., Kelly, M.E.M., Janero, D.R., Cascio, M. G., Stevenson, L.A., Pertwee, R.G., Kenakin, T.P., Denovan-Wright, E.M., Thakur, G. A., 2017. Enantiospecific allosteric modulation of cannabinoid 1 receptor. ACS Chem Neurosci. 8 (6), 1188–1203. https://doi.org/10.1021/acschemneuro.6b00310.

Hurst, D.P., Garai, S., Kulkarni, P.M., Schaffer, P.C., Reggio, P.H., Thakur, G.A., 2019. Identification of CB1 receptor allosteric sites using force-biased MMC simulated annealing and validation by structure–activity relationship studies. ACS Med. Chem. Lett. 10 (8), 1216–1221. https://doi.org/10.1021/acsmedchemlett.9b00256.

Shim, J.-.Y., 2009. Transmembrane helical domain of the cannabinoid CB1 receptor. Biophys. J. 96 (8), 3251–3262. https://doi.org/10.1016/j.bpj.2008.12.3934.

Lu, J., Byrne, N., Wang, J., Bricogne, G., Brown, F.K., Chobanian, H.R., Colletti, S.L., Di Salvo, J., Thomas-Fowlkes, B., Guo, Y., Hall, D.L., Hadix, J., Hastings, N.B., Hermes, J.D., Ho, T., Howard, A.D., Josien, H., Kornienko, M., Lumb, K.J., Miller, M. W., Patel, S.B., Pio, B., Plummer, C.W., Sherborne, B.S., Sheth, P., Souza, S., Tummala, S., Vonrhein, C., Webb, M., Allen, S.J., Johnston, J.M., Weinglass, A.B., Sharma, S., Soisson, S.M., 2017. Structural basis for the cooperative allosteric activation of the free fatty acid receptor GPR40. Nat. Struct. Mol. Biol. 24 (7), 570–577. https://doi.org/10.1038/nsmb.3417.

Morales, P., Goya, P., Jagerovic, N., Hernandez-Folgado, L., 2016. Allosteric modulators of the CB 1 cannabinoid receptor: a structural update review. CannabisCannabinoid Res. 1 (1), 22–30. https://doi.org/10.1089/can.2015.0005.

Tseng, C.-.C., Baillie, G., Donvito, G., Mustafa, M.A., Juola, S.E., Zanato, C., Massarenti, C., Dall'Angelo, S., Harrison, W.T.A., Lichtman, A.H., Ross, R.A., Zanda, M., Greig, I.R., 2019. The trifluoromethyl group as a bioisosteric replacement of the aliphatic nitro group in CB 1 receptor positive allosteric modulators. J. Med. Chem. 62 (10), 5049–5062. https://doi.org/10.1021/acs.jmedchem.9b00252.

Garai, S., Kulkarni, P.M., Schaffer, P.C., Leo, L.M., Brandt, A.L., Zagzoog, A, Black, T., Lin, X., Hurst, D.P., Janero, D.R., Abood, M.E., Zimmowitch, A., Straiker, A., Pertwee, R.G., Kelly, M., Szczesniak, A.-.M., Denovan-Wright, E.M., Mackie, K., Hohmann, A.G., Reggio, P.H., Laprairie, R.B., Thakur, G.A., 2020. Application of fluorine- and nitrogen-walk approaches: defining the structural and functional diversity of 2-phenylindole class of cannabinoid 1 receptor positive allosteric modulators. J. Med. Chem. 63 (2), 542–568. https://doi.org/10.1021/acs. jmedchem.9b01142.

Jakubík, J, El-Fakahany, E.E., 1953. Allosteric modulation of GPCRs of class a by cholesterol. Int. J. Mol. Sci. 22 (4) https://doi.org/10.3390/ijms22041953. **2021**.